ELSEVIER

Selection and Characterization of Saharan and Arabian Desert Sites for the Calibration of Optical Satellite Sensors

Hélène Cosnefroy, Marc Leroy,† and Xavier Briottet**

Desert areas are good candidates for the assessment of multitemporal, multiband, or multiangular calibration of optical satellite sensors. This article describes a selection procedure of desert sites in North Africa and Saudi Arabia, of size 100 × 100 km², using a criterion of spatial uniformity in a series of Meteosat-4 visible data. Twenty such sites are selected with a spatial uniformity better than 3% in relative value in a multitemporal series of cloud-free images. These sites are among the driest sites in the world. Their meteorological properties are here described in terms of cloud cover with ISCCP data and precipitation using data from a network of meteorological stations. Most of the selected sites are large sand seas, the geomorphology of which can be characterized with Spot data. The temporal stability of the spatially averaged reflectance of each selected site is investigated at seasonal and hourly time scales with multitemporal series of Meteosat-4 data. It is found that the temporal variations, of typical peak-to-peak amplitude 8–15% in relative value, are mostly controlled by directional effects. Once the directional effects are removed, the residual rms variations, representative of random temporal variability, are on the order of 1–2% in relative value. The suitability of use of these selected sites in routine operational calibration procedures is briefly discussed.

INTRODUCTION

Physical measurements of the Earth surface plus atmosphere system can be derived from satellite sensors provided that their calibration procedures are sufficiently accurate. Many present or forthcoming sensors are equipped with onboard calibration devices. However, a key issue for the assessment of calibration accuracy and reliability is the ability to intercompare several independent sources of estimation of the calibration coefficients. This is why it is particularly important to develop alternative calibration methods based on the viewing of well-characterized test sites (e.g., Slater et al., 1987). In the solar reflected spectrum, such a development is critically important for the use of sensors such as AVHRR[1] / NOAA[2], Meteosat, or POLDER[3] / ADEOS[4] (Deschamps et al., 1994), which are not equipped with onboard calibration devices.

Stable desert areas of Sahara and Saudi Arabia can potentially be used as calibration test sites in the solar reflected spectrum. Such sites have in fact already been used to monitor the calibration temporal drifts of the AVHRR (Holben et al., 1990; Staylor, 1990; Santer et al., 1991; Kaufman and Holben, 1993; Santer and Roger, 1993; Cabot et al., 1994), Meteosat (Dedieu, 1992; Cabot et al., 1994) and HRV[5] / Spot sensors (Henry et al., 1993). It is in fact conceivable to consider the use of stable desert areas not only for multitemporal calibration purposes, but also for an evaluation of the multiangular calibration of wide field of view sensors equipped with charge coupled device (CCD) detectors, such as POLDER / ADEOS, Vegetation / Spot4, MISR[6] / EOS[7], or MERIS[8] / Envisat (Delphin et al., 1991). This requires that the sites be well characterized

*CERT-DERO, Toulouse, France
†CESBIO, UMR CNES-CNRS-UPS, Toulouse, France

Address correspondence to Xavier Briottet, ONERA / CERT / DERO, 2, av. E. Belin, 31055 Toulouse Cedex, France.
Received 4 April 1995; revised 23 August 1995.

[1] Advanced Very High Resolution Radiometer.
[2] National Oceanic and Atmospheric Administration.
[3] POLarization and Directionality of Earth's Reflectances.
[4] ADvanced Earth Observing System.
[5] Haute Résolution dans le Visible.
[6] Multi Angle Imaging Spectroradiometer.
[7] Earth Observing System.
[8] MEdium Resolution Imaging Spectrometer.

REMOTE SENS. ENVIRON. 58:101–114 (1996)

655 Avenue of the Americas, New York, NY 10010

0034-4257 / 96 / $15.00
SSDI 0034-4257(95)00211-1

in terms of directional variations of their top of the atmosphere (TOA) reflectances, to account for variations of the solar or viewing configurations between measurements. A third objective could be the assessment of multiband calibration of optical sensors. For this an *a priori* knowledge of the spectral variations of the sites TOA reflectances is needed.

One can identify two basic steps of the methodological development of operational calibration procedures using desert test sites. First, it is necessary to select and characterize a number of candidate calibration sites, on the basis of criteria such as spatial uniformity, temporal stability at all scales between hours and tens of years, magnitude of directional effects, and cloud cover. The size of the chosen sites must be compatible with the size of pixels of coarse resolution sensors such as POLDER / ADEOS or Vegetation / Spot4. Second, one needs to perform metrological measurements of the spatially averaged bidirectional spectral TOA reflectance of each of the selected sites. This reflectance, which may be called reference or calibrated reflectance, may be denoted by $\rho\ (\lambda, \theta_S, \theta_V, \varphi)$ that is, a function of wavelength λ, Sun and view zenith angles θ_S and θ_V, and relative azimuth φ between Sun and view directions. The metrological evaluation of this reflectance does not need to be performed during the overpass of the satellite sensor to be calibrated, provided that the surface and the atmosphere of the selected test site are sufficiently stable. It can be derived in fact much before this, using satellite, airborne, and ground reference data, possibly coupled to some modeling to extrapolate measured reflectances to a range of wavelengths and Sun and view directions not obtained during the experimental measurements.

Sensor calibration may be inferred from the comparison between the reference reflectance and measurements of the satellite sensor. For example, the multiangular calibration of a wide field of view sensor may be achieved by comparing successive satellite acquisitions of one site, taken with different viewing angles, during a relatively short period (typically one month). The comparison of the ratios x(site, $t1$) / x(site, $t2$) and ρ(site, Sun and view angles at $t1$) / ρ(site, Sun and view angles at $t2$), where x(site, t) refers to the satellite digital measurement at time t spatially averaged over the site, provides the desired intercalibration between two different groups of detectors in the sensor focal plane. The test sites should be as numerous as possible and cover a relatively extended region of the world to calibrate efficiently the entire focal plane in a reasonable amount of time. A multitemporal calibration can be performed using a similar principle. It can be derived through a comparison of successive measurements over one site with the same viewing angle, possibly separated by a large period of time, and through the use of the reference reflectance to account for variations of Sun zenith angle and azimuth between measurements. Finally, multiband calibration is rather straightforward and can be acquired with one satellite overpass over one site, using the knowledge of the spectral variations of the site reference reflectance.

This calibration principle is different from currently applied calibration procedures on test sites, such as those of White Sands (e.g., Slater et al., 1987; Teillet et al., 1990) or La Crau (Santer et al., 1992), where it is critically important to perform ground measurements of the surface and atmosphere properties *during* the satellite overpass. This is important because the natural temporal variability of site reflectances exceeds by far the level of calibration accuracy which is desired (in the range 2–5%). For example, Wheeler et al. (1994) show that the albedo of the Alkali Flats region in the White Sands area is highly influenced by surface moisture conditions and can vary in time by as much as 30%. By contrast, the basis of the present approach is to locate regions in the world, the optical properties of which are sufficiently stable so that *in situ* measurements simultaneous to the satellite overpass can be avoided.

This article documents the results of a selection and characterization procedure of 20 100×100 km^2 desert sites of Saharan North Africa and Saudi Arabia. The size of the sites (100 km) has been chosen to be easily tractable with POLDER data (pixel size ~ 7 km). This size is *a fortiori* compatible with calibration needs of sensors of finer spatial resolution, such as AVHRR, Vegetation / Spot4, or even with multitemporal calibration needs of TM[9] / Landsat or HRV / Spot, provided sensor measurements be spatially averaged over a sufficiently large area in the selected site. The site selection is based on a criterion of spatial uniformity using a multitemporal series of Meteosat-4 data. The selected sites are then characterized in terms of cloud cover using International Satellite Cloud Climatology Project (ISCCP) data, precipitation using data from a network of meteorological stations, geomorphology using HRV / Spot data, and temporal stability and directional effects at hour and seasonal time scales using multitemporal series of Meteosat-4 data.

SELECTION OF DESERT SITES

The selection process is based on a spatial uniformity criterion. It is made with three Meteosat-4 images per month, taken at 9 h 30 min UT, from July to November 1989, that is, a total of 15 different images. The images are taken at full resolution (2.5 km at nadir) in the visible channel, and are coded on 8 bits per pixel. A crude cloud mask is drawn interactively on each image by visual inspection. For cloud-screened pixels, the 8-bit

[9] Thematic Mapper.

Figure 1. Map of relative spatial uniformity $\sigma(\rho)/\rho$ (see text for explanations) at Meteosat resolution over North Africa and Saudi Arabia, on 25 July 1989. White squares correspond to the selected sites.

digital counts C, corrected for offset term, are transformed into reflectance values ρ according to the relation

$$\rho = \frac{\pi KC}{E \cos \theta_s}, \qquad (1)$$

where K is a calibration coefficient, and E is the TOA normal solar irradiance averaged over the Meteosat-4 visible band, corrected for the Earth–Sun distance on the date of observation. [More precisely, $E = \int E(\lambda)S(\lambda)\, d\lambda$, where $E(\lambda)$ is the spectral solar irradiance and $S(\lambda)$ is the dimensionless spectral sensitivity of the visible band of Meteosat-4, normalized so that its maximum for all wavelengths equals unity.] In our work we have retained the value $K = 1.08$ W m^{-2} sr^{-1} per 8-bit count, recommended for desert scenes by Kriebel and Amann (1993). Images are subsequently processed to produce images of $\sigma(\rho)/\rho$ at the same resolution as the original images. Here $\sigma(\rho)$ and ρ stand, respectively, for each current pixel, for the standard deviation of reflectances evaluated in a sliding window 41×41 pixels (about 100×100 km^2) around the current pixel, and for the average reflectance in this window. Figure 1 is an example of an image of relative spatial uniformity $\sigma(\rho)/\rho$. A site is selected whenever the relative spatial uniformity associated with its central pixel is found to be less than 3% in all cloud screened images of our data set.

Twenty different sites have been selected using this method. They are indicated on a map in Figure 2. The coordinates in latitude and longitude of the center of each site are reported in Table 1 (columns a and b). As can be seen in Figure 2 or Table 1, five sites are located in Algeria, one in Egypt, four in Libya, three in Niger, one in Sudan, one in Mali, two in Mauritania, and three in Saudi Arabia. Note that the sites Libya 1–4 and Egypt 1 are very close to three out of the four Saharan sites that have been selected by Kaufman and Holben (1993). Also, the sites Libya 2, 3, 4, Egypt 1, and Sudan 1 are included in the $10° \times 10°$ area selected by Staylor (1990).

A systematic assessment of spatial uniformity is then made on a larger data set, consisting of cloud screened Meteosat-4 images acquired at 9 h 30 min UT every second day from July 1989 to January 1990. Table 1 (columns c, d, and e) reports, in relative value and for each selected site, the minimum, time-averaged, and maximum spatial uniformity performance found by exploring the totality of this data set. The time averaged spatial uniformity ranges from 1% to 2.6% depending on the selected site. The time variability of this performance is generally small, the differences between maximum and minimum spatial uniformities being less than 1% for 17 sites out of 20.

Ideally the selection should be such as to select sites in desert areas that satisfy simultaneously several criteria: good spatial uniformity and temporal stability at all length and time scales, minimum directional variations, minimum cloud cover, and minimum atmospheric variabilities associated with changes of aerosols and water vapor amounts. This would be very difficult in practice since the areas under investigation (North Africa and Saudi Arabia) are quite extended. Therefore, for reasons of practicability, we have chosen to privilege the spatial uniformity criterion, conjecturing that if a site is repeatedly very uniform over a large period of time, it is quite likely that it should satisfy the other criteria as well. This conjecture has been partly verified with three selected sites (Libya 4, Sudan 1, and Egypt 1), with a verification that these sites are more stable than their surrounding regions, at least on a time scale of a few days to a week. To demonstrate this, eight

Table 1. Site Locations and Relative Spatial Uniformity (%) (See Text)

Site Location			*Spatial Uniformity*		
Site Name	*Latitude (deg) a*	*Longitude (deg) b*	*Averaged over Time (%) c*	*Maximum (%) d*	*Minimum (%) e*
Arabia 1	18.88	46.76	1.6	2.8	1.0
Arabia 2	20.13	50.96	1.6	3.2	0.90
Arabia 3	28.92	43.73	2.0	2.5	1.9
Sudan 1	21.74	28.22	1.8	2.2	1.7
Niger 1	19.67	9.81	2.0	2.4	1.7
Niger 2	21.37	10.59	2.1	2.3	1.6
Niger 3	21.57	7.96	2.6	3.1	2.2
Egypt 1	27.12	26.10	1.3	1.7	1.0
Libya 1	24.42	13.35	2.1	2.6	1.9
Libya 2	25.05	20.48	1.6	2.2	1.2
Libya 3	23.15	23.10	2.7	2.9	2.4
Libya 4	28.55	23.39	1.3	1.8	1.0
Algeria 1	23.80	−0.40	1.6	2.0	1.2
Algeria 2	26.09	−1.38	1.5	1.8	1.3
Algeria 3	30.32	7.66	1.2	2.5	0.84
Algeria 4	30.04	5.59	1.7	2.2	1.3
Algeria 5	31.02	2.23	1.7	2.4	1.2
Mali 1	19.12	−4.85	0.96	1.5	0.7
Mauritania 1	19.40	−9.30	1.7	2.2	1.3
Mauritania 2	20.85	−8.78	2.2	2.6	1.7

Figure 2. Site locations on a map.

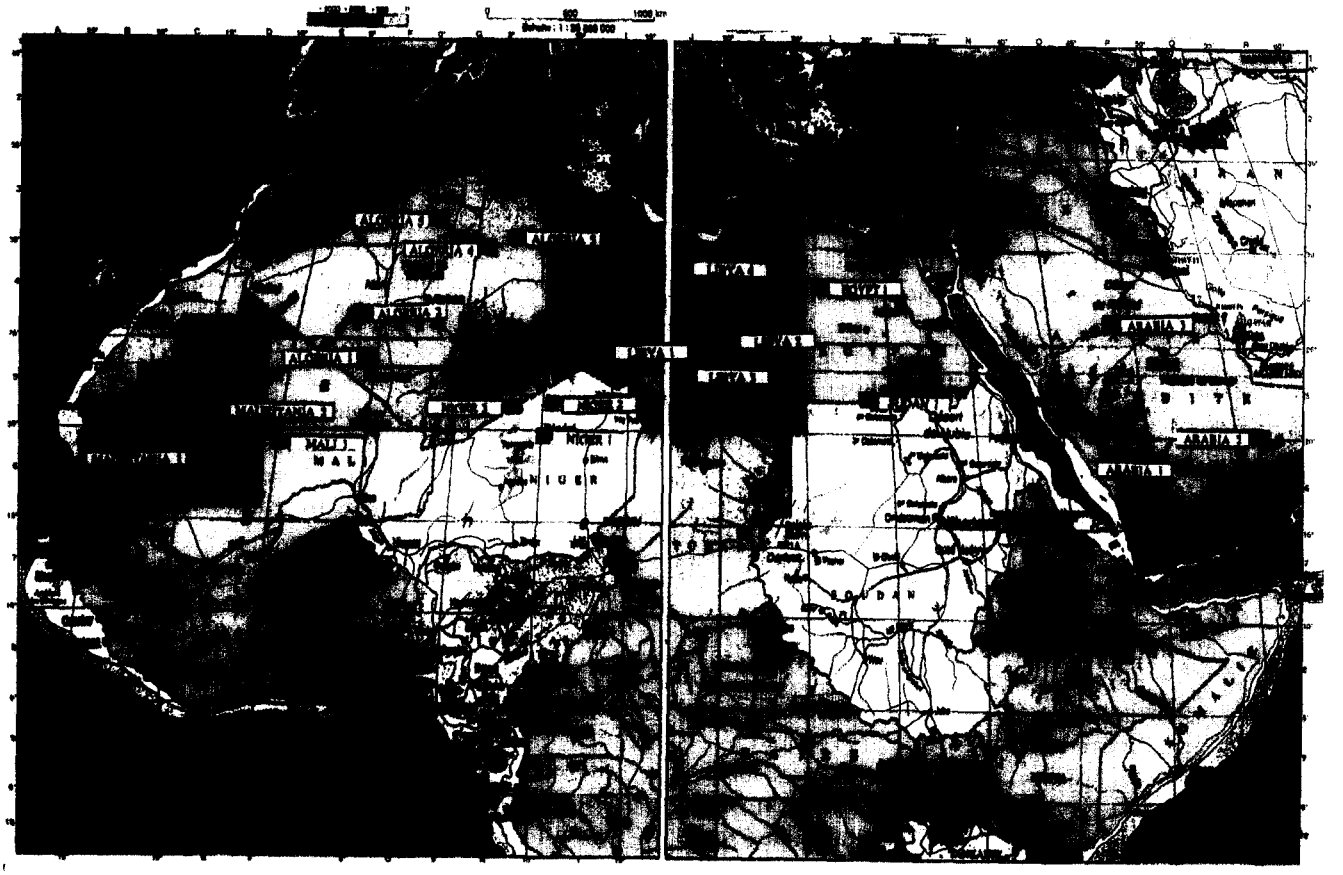

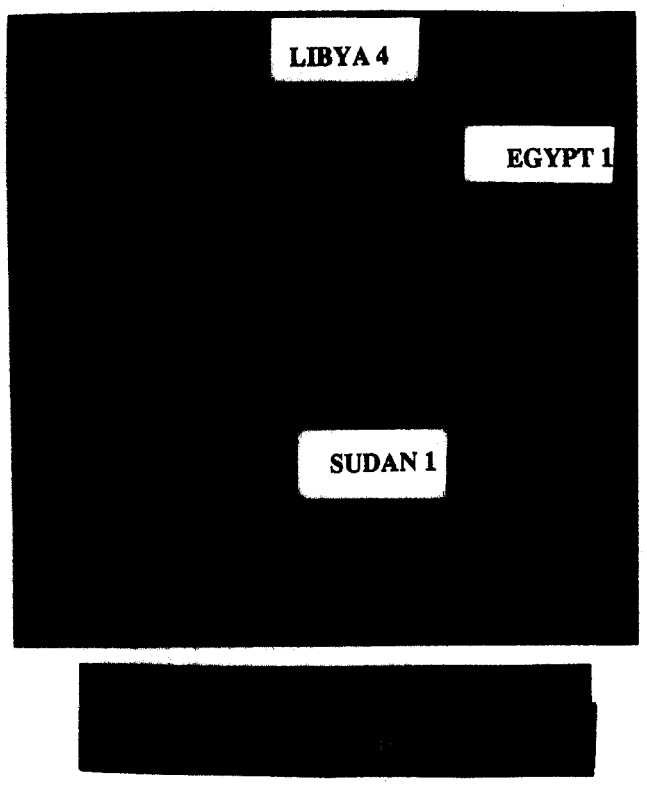

Figure 3. Image of standard deviation (%) of temporal variations of Meteosat reflectance over 15 days, normalized by time averaged reflectance, for a region in Libya, Sudan, and Egypt.

Meteosat-4 images, taken at 9 h 30 min UT every second day from 15 to 29 July 1989, were processed for a region about 1000 km in size in Libya, Egypt and Sudan, with a selection of *a priori* flat and desertic regions, completely cloud-free in all eight images. The images were transformed in TOA reflectances using Eq. (1), registered to each other using ground control points, and smoothed with a 3×3 pixel averaging filter to minimize residual misregistration effects. For each pixel of this region, the standard deviation of the temporal variation of the pixel reflectances for the ensemble of eight dates was computed and normalized by its time averaged reflectance. The resultant image is shown in Figure 3, on which the selected sites Libya 4, Sudan 1, and Egypt 1 are indicated. Figure 3 shows that our selected sites correspond effectively to the most stable areas of the region, with a temporal stability performance of typically 1–1.5%.

CLOUD COVER AND PRECIPITATION

Cloud cover statistics on selected sites have been studied using the so-called C1 data from the International Satellite Cloud Climatology Project (ISCCP) (Schiffer and Rossow, 1983; Rossow et al., 1988; Rossow and Schiffer, 1991), and provided to us by Laboratoire de Météorologie Dynamique, in Palaiseau (France). These data document for the whole Earth, at a resolution of 280×280 km^2, at different local times, the complete statistics on cloud coverage on periods ranging from a month to several years. The ISCCP data are constructed by applying cloud detection algorithms to a compilation of meteorological satellite data such as AVHRR, GOES,[10] or Meteosat. The ISCCP C1 data have been shown to be reasonably accurate in desert regions (Capderou and Kandel, 1994). They have been used to infer, for each selected site (located in a given 280×280 km^2 C1 "pixel"), the percentage of days in a month for which the cloud cover fraction (i.e., the area declared cloudy in the C1 pixel, divided by the total area of this pixel) is less than 10%. These monthly percentages have been averaged for data from 1983 to 1987.

The results are illustrated in Figure 4, which shows for four representative sites, from west to east, Mali 1, Algeria 2, Libya 4, and Arabia 2, the histograms of percentage of clear days in a month ("clear day" being understood here as a day with cloud cover fraction less than 10%) as a function of the month in the year, at a local time of 10 h 30 min. A compilation of similar results for each of the 20 selected sites is also shown in Table 2. Figure 4 and Table 2 show that the percentage of clear days vary according to the site location and also seasonally, from a few percents in the Western sites in winter, to more than 90% in Libyan sites in summer. The yearly averaged cloud cover performance varies from 20–30% for the Mali and Mauritania sites, to 40–60% for the other sites. The clearest sites are those of Libya, Arabia, Egypt and Sudan (Table 2). Some seasonal variations of cloud cover do exist (Fig. 4, Table 2), but the magnitude of these variations is moderate and all selected sites could be used during the whole year for calibration purposes.

Precipitation data are also useful to assess the quality of the selected sites. The probability that the selected site remains stable in time is enhanced when the precipitation is low, while sizeable precipitation is generally associated with onsets of vegetation activity, which can affect the site reflectance properties. We have compiled precipitation data from the Global Historical Climatology Network database (Vose et al., 1992), from which it is possible to extract monthly precipitation estimates recorded in a network of local stations neighboring our sites in Sahara and Saudi Arabia, averaged over long periods of time (from 40 years to 100 years). These data provide interesting orders of magnitude, although they represent quite probably upper limits of the actual precipitation in our selected sites, the distance between site center and local station being usually very large, on the order of 100–400 km depending on the site. Examples of such data are included in Figure 4 with the

[10] Geostationary Operational Environmental Satellite.

Table 2. Percentage of Clear Days in a 3-Month Period and Yearly Average Percentage of Clear Days (at 10 h 30 min Local Time) for Each Selected Site[a]

	Percentage Clear Days (%)					*Average Monthly Precipitation (mm)*				
Site	*Jan.–Mar.*	*Apr.–Jun.*	*Jul.–Sep.*	*Oct.–Dec.*	*Year*	*Jan.–Mar.*	*Apr.–Jun.*	*Jul.–Sep.*	*Oct.–Dec.*	*Year*
Arabia 1	58	49	54	79	60	18.2	7.7	0	14.4	10.1
Arabia 2	52	50	60	76	60	18.2	7.7	0	14.4	10.1
Arabia 3	42	47	85	46	55	12.7	5.1	0	15.9	8.4
Sudan 1	58	71	81	66	69	0.1	0.3	0.3	0.2	0.2
Niger 1	41	56	43	48	47	0.1	0.5	0.8	0.5	0.5
Niger 2	38	59	75	52	56	0.1	0.5	0.8	0.5	0.5
Niger 3	41	53	60	52	51	3	1.9	1	1.7	1.9
Egypt 1	45	63	92	60	65	0.6	0.3	0.1	0.5	0.4
Libya 1	30	58	86	45	55	2	0.7	0.7	2.4	1.4
Libya 2	46	65	92	61	66	0	0.3	0	0.2	0.1
Libya 3	46	71	89	66	68	0.3	0.1	0.1	0.1	0.2
Libya 4	44	60	92	39	59	1.2	0.6	0.1	1.2	0.8
Algeria 1	44	44	44	41	43	1.9	0.7	2.5	1.3	1.6
Algeria 2	52	39	58	49	49	2.2	2	2	2.6	2.2
Algeria 3	47	39	69	39	48	4.4	1.5	0.5	5	2.8
Algeria 4	51	42	65	41	50	3.2	1.4	0.4	3.9	2.2
Algeria 5	48	41	59	44	48	5.8	1.4	0.8	6.5	3.6
Mali 1	28	38	20	23	27	1.3	1.7	11	2.4	4.1
Mauritania 1	26	34	24	17	25	1.9	0.9	11.8	4.8	4.8
Mauritania 2	37	43	35	34	37	1.9	0.9	11.8	4.8	4.8

[a] Also, the same with monthly precipitation (mm) instead of percentage of clear days.

cloud cover data of the four sites mentioned above. A compilation of similar results for each of the 20 selected sites, at a 3-month temporal resolution, is also shown in Table 2. Figure 4 and Table 2 show that all sites have at least one season when the monthly precipitation is extremely small, less than 2 mm / month. The dryest season is spring for the western sites, and summer for the eastern sites of Arabia. The sites of Sudan, Egypt, Libya, and Niger are dry all year long, with average monthly precipitation from 0.1 mm / month to 1.9 mm / month depending on the site. Some correlation exists as expected between increases of precipitation and increases of cloud cover.

GEOMORPHOLOGY

Most of selected sites belong to the category of large systems of sand dunes, with a few exceptions (Sudan 1, Libya 3, Niger 3, Algeria 1). The use of images of high spatial resolution sensors such as HRV / Spot or TM / Landsat turns out to be quite adequate to investigate the fine structure of the sites (Jaccoberger, 1989; Cooke et al., 1993). This is useful to characterize spatial inhomogeneity at a finer scale than that of Meteosat, in terms of measured radiance but also in terms of land cover. This is also useful to characterize the relief structure, which is important information, since relief can modify the directional signature of reflectance measured from space, and thus affect the measurement of the site reference reflectance mentioned in the introduction. HRV / Spot images were acquired and processed for 11 out of 20 selected sites. A sample of six of these 11 images, in the red HRV / Spot channel (XS2), is represented in Figure 5, which provides, in our view, a fairly representative subset of the various situations which can be encountered. The images of Figure 5 represent areas of 20×20 km^2 inside the 100×100 km^2 selected areas. A 20×20 km^2 area generally represents well the total area of a site (recall that the sites have been chosen with a criterion of good uniformity). With the exception of the Sudan 1 site (Fig. 5f), mostly stony, these images show periodic and reproducible sand dune patterns. The variations of radiometry seen on these images are interpretable essentially in terms of local variations of solar irradiance, which is mainly proportional to the cosine between local normals to the surface and the solar direction. Thus these images provide a fairly good description of relief, or at least of horizontal dimensions of the dune structures. Note that as expected the images show no trace of vegetation.

The geomorphological structure of desert sand dunes has been studied for years (see the review by Cooke et al., 1993). According to existing sand dune classifications (Cooke et al., 1993; Mainguet, 1984), the sand dunes of Figures 5 a–c (Algeria 2, Egypt 1, and Libya 1), Figure 5d (Niger 2), and Figure 5e (Algeria 3) may be classified as linear, transverse and star dunes, respectively. As can be seen in Figure 5, the interdune distance varies from a few hundred meters (Niger 2) to 2–3 km (Algeria 2, for example). The longitudinal dimension of linear dunes can be quite large, from several kilometers to several tens of kilometers (Figs. 5 a–c). The transverse dimension of dunes varies from typically 100 m (Niger 2 and Libya 1) to 1 km (Algeria

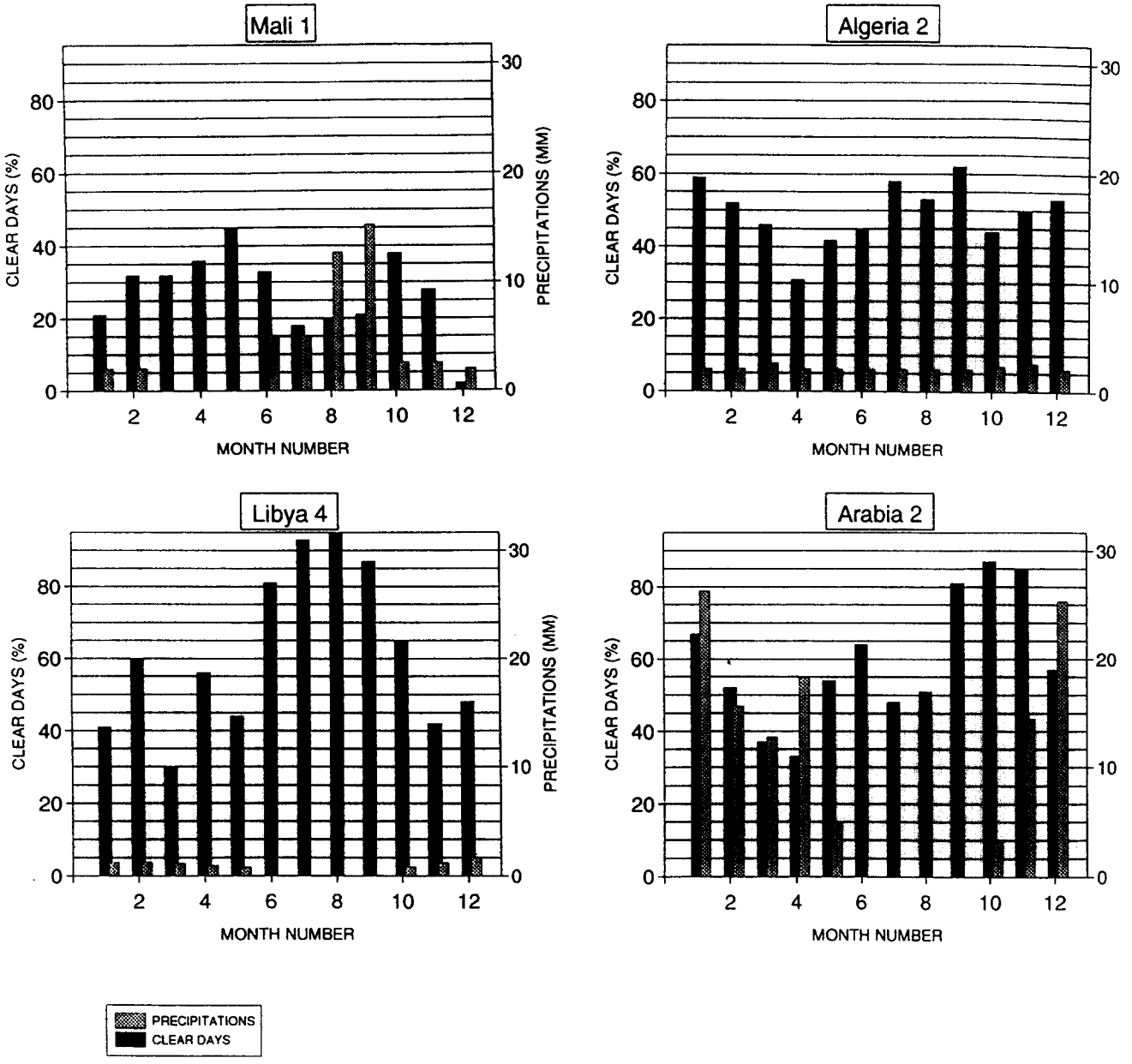

Figure 4. Dark bars: average percentage of clear days in a month (%) as a function of the number of the month in the year, at a local time of 10 h 30 min, for four representative sites. Grey bars: with the same abcissae, average precipitation (mm) in a month.

2 and Algeria 3). The height of dunes cannot be directly inferred from the Spot images, but is known to vary typically from about 10 m (Libya 1 and Niger 2) to 100 m (Algeria 2 and Algeria 3) (Cooke et al., 1993; Cosnefroy et al., 1996).

TEMPORAL STABILITY AND DIRECTIONAL EFFECTS

In the following, a systematic investigation of temporal stability performances is made for all selected sites, at seasonal and at hour time scales, using Meteosat-4 satellite time series. In order to discriminate between "true" temporal variability and directional effects due to changes in time of the Sun position (recall that for geostationary satellites the viewing direction for any given site is fixed), the satellite time series are adjusted against a model of TOA bidirectional reflectance, and the "true" time variability is deduced by difference between observed and modelled data.

Seasonal Time Scale

The seasonal variations of all selected sites have been investigated with full (2.5 km) resolution Meteosat-4 visible images acquired at 9 h 30 min UT every second day during the period from July 1989 to January 1990

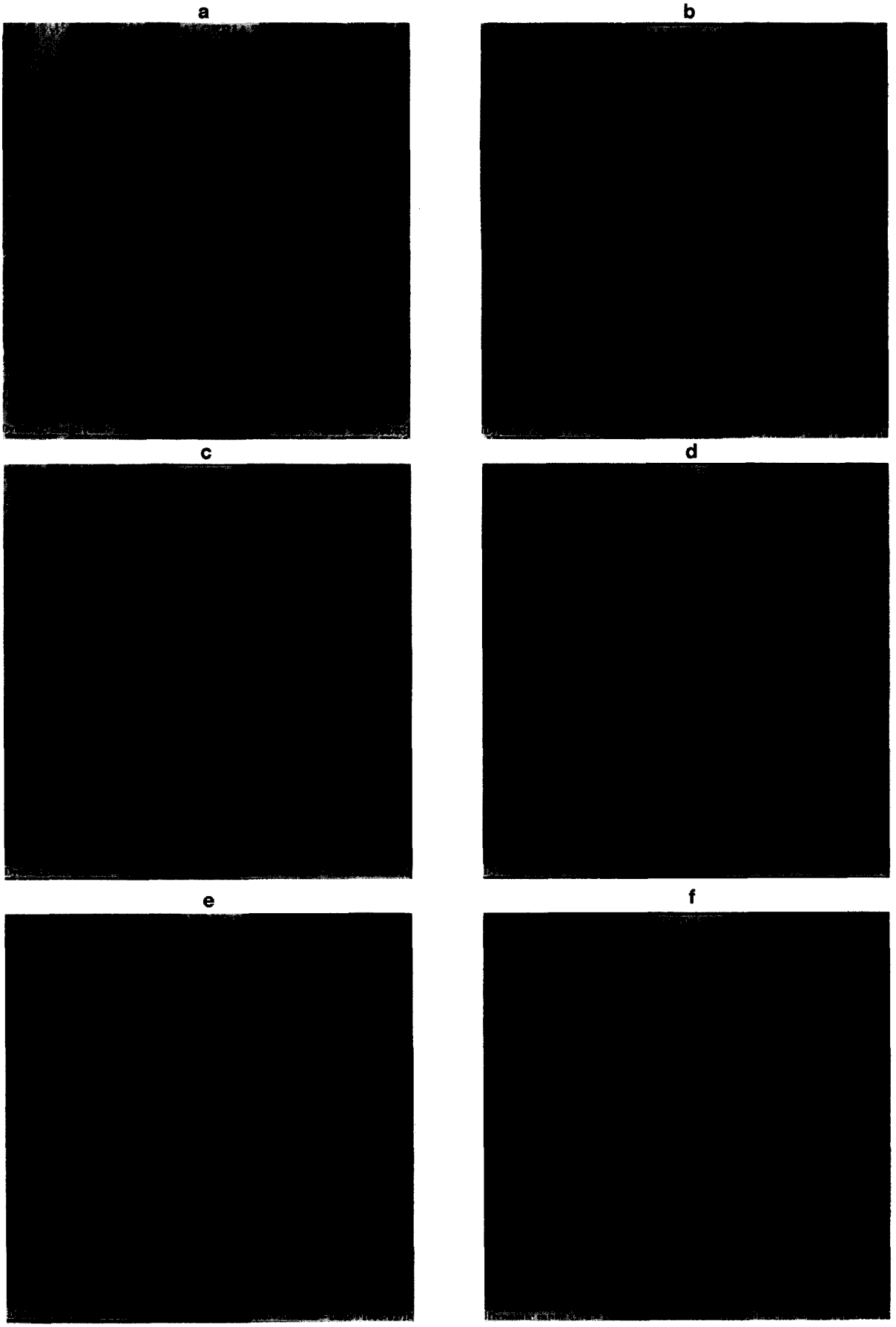
a
b
c
d
e
f

(92 images). This seasonal data set is believed to be representative of any seasonal data that could be acquired on these sites. This statement is supported by studies done with a multiannual ISCCP-B2 Meteosat data set, at space and time resolutions of 30 km and 10 days, which show that the seasonal variations on a Libyan desert site (close to Libya 1) are very much alike from one year to another (Gastineau, 1991).

Cloud screening is a critical processing step in the determination of temporal variations of reflectances. Many different algorithms exist for cloud cover detection (e.g., Rossow, 1989). Most of these algorithms use a combination of visible and thermal infrared thresholds, based on the principles that clouds are usually brighter in the visible, and colder in the thermal infrared, than the underlying surface. Such algorithms are applied, or example, to produce ISCCP C1 data. However, visible threshold techniques are less suited to desert areas due to their large brightness. Capderou and Kandel (1994) have proposed to sharpen these criteria through the analysis of the space and time variability of the directional signature of site reflectances. We propose a different approach here, which takes advantage of the fact that our sites have a very good spatial uniformity, and that cloud cover is expected to be very inhomogeneous on desertic areas. For each site and each date, three TOA reflectances ρ_{max}, ρ_{min}, and ρ have been computed. Here ρ_{max}, ρ_{min}, and ρ stand respectively for the maximum and minimum reflectances found by exploring the entire site, and the spatially averaged reflectance of the site. Figure 6 gives a representative example of the time variations of these three quantities for the particular site Niger 1. One can see the appearance of peaks in ρ_{max}, correlated with valleys in ρ_{min}, and to a lesser extent correlated with moderate peaks in ρ. These peaks and valleys are related to cloud occurence, since any appearance of clouds results in a large increase of ρ_{max}, due to cloud brightness, and to an associated decrease of ρ_{min} due to cloud shadow effects. The cloud screening technique that we have adopted has thus been to apply systematically, on all data, a threshold on the quantity $(\rho_{max} - \rho_{min})/\rho$. This technique has the advantage that it can be used operationally with sensors not equipped with thermal infrared channels, such as Vegetation / Spot4 or POLDER / ADEOS. Note that the variations with site location of the number of cloud-free data derived with this method (see Table 3, column d) are generally consistent with the results of cloud cover derived from the ISCCP C1 data (Table 2).

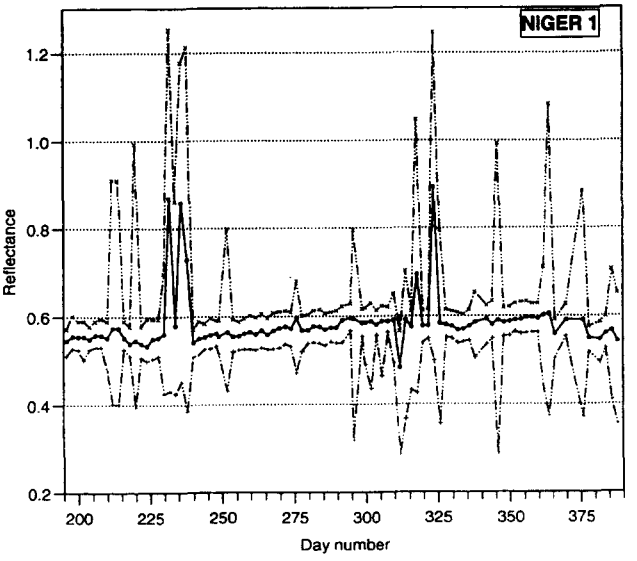

Figure 6. Seasonal evolution of spatially averaged TOA reflectance (full line), maximum and minimum reflectances (dotted lines) for site Niger 1. Day number refers to the day number starting from 1 January 1989.

Figure 7 presents the time variations of the spatially averaged reflectance ρ, after cloud screening, for the four sites Niger 1, Niger 3, Mauritania 2, and Libya 1 taken as representative examples. Figure 7 shows short-term variations of rather small amplitude (a few percent in relative value), superimposed on low frequency seasonal variations of sizeable amplitude with rather similar characteristics for the four sites. While the short-term variations are interpreted as temporal instability effects (due to some surface or atmospheric variability), the seasonal variations are interpreted as directional reflectance effects related to the seasonal variations of Sun position, as in Delphin et al. (1991) or Cabot et al. (1994). Table 3 (column a) provides for all selected sites the peak-to-peak amplitude, in relative value, of the time variations of ρ (cloud screened data) for the entire period from July 1989 to January 1990. The peak-to-peak amplitude of seasonal variations found in Table 3, generally on the order of 10–15% in relative value, is consistent with earlier results (Delphin et al., 1991), where similar variations were found when comparing AVHRR data with widely varying view angles on desertic areas during a NOAA orbital cycle, that is, about 10 days. Higher numbers are obtained for the Arabian sites (up to 23%). This is interpreted as a consequence of their longer distance from the subsatel-

Figure 5. HRV / SPOT images, channel XS2, for 20×20 km^2 areas at six selected sites. Annotation in each frame indicates the position (latitude, longitude) of the center of the image, and the lower and upper limits in digital counts of the dynamic range from black to white.

Table 3. Temporal Stability and Directional Effects of Each Site (See Text)

	Seasonal Variations				*Hourly Variations*				*Comparison Seasonal/Hourly Models (rms differences) (%) i*
Site	*Peak-to-Peak (%) a*	*rms of Fit (%) b*	R^2 *c*	*Number Cloud-Free Data d*	*Peak-to-Peak (%) e*	*rms of Fit (%) f*	R^2 *g*	*Number Cloud-Free Data h*	
Arabia 1	14	1.8	0.84	51	40	2.2	0.98	9	3.4
Arabia 2	20	1.6	0.91	56	53	0.8	1.0	10	3.7
Arabia 3	23	1.8	0.92	48	–	–	–	2	–
Sudan 1	12	1.4	0.84	74	–	–	–	2	–
Niger 1	10	1.7	0.62	60	7	1.6	0.49	11	0.7
Niger 2	7	1.3	0.83	56	13	1.8	0.79	11	0.2
Niger 3	11	1.3	0.83	66	11	1.5	0.79	11	0.9
Egypt 1	12	1.1	0.90	76	14	0.7	0.98	9	0.8
Libya 1	10	1.2	0.82	70	6	1.4	0.71	10	0.2
Libya 2	12	1.4	0.84	76	–	–	–	0	–
Libya 3	11	1.2	0.89	74	19	1.4	0.95	11	0.3
Libya 4	13	1.2	0.92	71	9	0.5	0.97	5	0.9
Algeria 1	12	1.6	0.73	54	5	0.7	0.81	10	4.5
Algeria 2	13	1.4	0.86	47	4	0.6	0.74	7	0.8
Algeria 3	15	1.5	0.90	40	11	0.9	0.92	10	0.3
Algeria 4	14	1.3	0.92	50	5	0.6	0.85	7	0.7
Algeria 5	17	1.6	0.90	37	5	0.6	0.78	7	6.1
Mali 1	10	1.8	0.67	30	5	1.0	0.66	11	0.8
Mauritania 1	13	2.8	0.43	35	11	1.3	0.80	11	0.7
Mauritania 2	13	2.0	0.50	41	12	1.2	0.88	11	0.1

lite point. Their view zenith angle (about 60°) is larger than that of the Saharan Sites (about 25–40°) and the directional effects are therefore expected to have a higher amplitude (e.g., Kimes, 1983; Cosnefroy et al., 1996).

Thus, the ultimate performance of desertic areas in terms of temporal stability at seasonal time scales should be evaluated by removing the variations due to directional effects. To do this, we apply a regression between time profiles of ρ obtained at the previous step and the 4-parameter bidirectional reflectance model of Staylor and Suttles (1986), derived in the context of radiative budget analysis on desertic areas. This model reads

$$\rho(\theta_s, \theta_v, \varphi) = \frac{1}{\cos\theta_s \cos\theta_V}\left[Y_0 + Y_1\left(\frac{\cos\theta_s \cos\theta_V}{\cos\theta_s + \cos\theta_V}\right)^N\right] \times \frac{(1 + C_{sw}\cos^2\xi)}{1 + C_{sw}[\cos^2\theta_s \cos^2\theta_V + (\sin^2\theta_s \sin^2\theta_V)/2]}, \quad (2)$$

where Y_0, Y_1, N, and C_{sw} are the model parameters and where ξ is the phase angle, related to the Sun and view zenith angles θ_S and θ_V, and to the relative azimuth between Sun and view directions φ by

$$\cos\xi = \cos\theta_s \cos\theta_v + \sin\theta_s \sin\theta_v \cos\varphi. \quad (3)$$

Table 3 gives for each site the rms of fit (column b) resulting from this regression, expressed in relative value (that is, the rms difference between modeled and observed reflectances, normalized by the time averaged ρ), the determination coefficient R^2 of this regression (column c), and the number of cloud-free data used in the regression (column d). Table 3 shows that the correlation is good, with R^2 coefficients generally higher than 0.8, and that the rms of fit is generally on the order of 1–2%. As said above, the rms of fit is interpreted as the performance of random temporal variability of the selected sites, while the low frequency part of the temporal variations is assumed to be due to directional effects, modeled by Eq. (2). This conjecture is supported by the analysis performed at the end of this section (comparison between hourly and seasonal data sets).

The best performances of temporal stability are obtained for the Egypt and Libya sites, which correspond also to sites with very small cloud cover (see previous Section). The higher rms of fit (2% and 2.8%) and mediocre R^2 coefficients (less than 0.5) obtained in the case of the Mauritania sites are interpreted as a consequence of relatively poor cloud cover conditions on these sites.

Hour Time Scale

The hourly variations of site reflectance have been studied with 1 full resolution visible Meteosat-4 image per hour from 4 h UT to 17 h UT, for a particular date, 30 September 1989. Only data for which θ_S is less than 80° were included. The time evolution of the spatially averaged TOA reflectance ρ of each site has been derived exactly as in the previous subsection.

Figure 8 represents the hourly time evolution of ρ

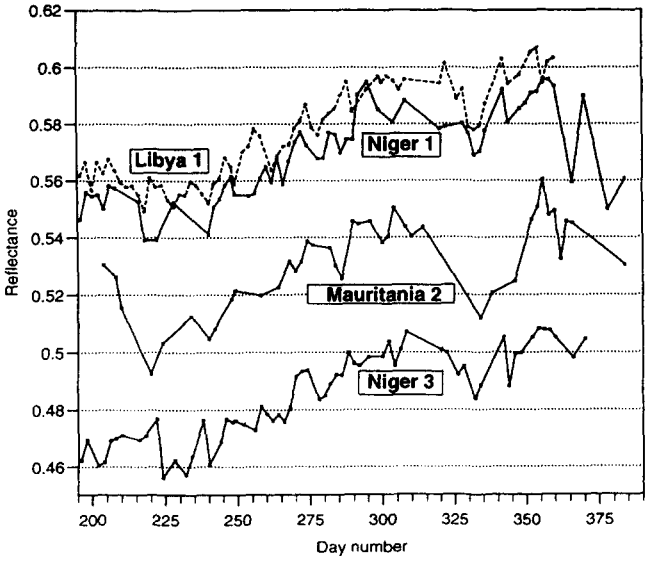

Figure 7. Seasonal evolution of spatially averaged TOA reflectance of four different sites. Day number refers to the day number starting from 1 January 1989.

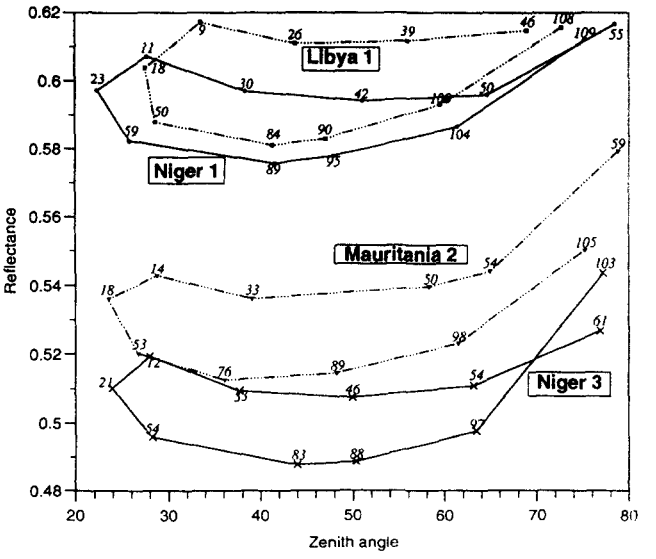

Figure 8. Hourly evolution of spatially averaged TOA reflectances on 30 September 1989 for four different sites (same as Fig. 7), plotted as a function of solar zenith angle (deg). Successive data are linked together for readability. Numbers associated with each data point are relative azimuths between solar and view directions (deg).

for the four sites Niger 1, Niger 3, Libya 1, and Mauritania 2 (the same as for Fig. 7). Time in the abscissa axis has been replaced by the Sun zenith angle θ_S, and each data point is labeled with the corresponding relative azimuth φ. The behavior of ρ is very similar for the four sites with a smooth and steady evolution, with relatively higher reflectances for high θ_S (in the morning and in the evening), and with a peak-to-peak relative amplitude of variations of about 6–12%. These variations, on the same order of magnitude as seasonal variations studied in the previous paragraph, provide additional evidence that the temporal variations of reflectance are mostly controlled by directional effects associated to variations of the Sun's position. Table 3 (column e) gives the peak-to-peak amplitude of variations of reflectance on 30 September 1989 for each site, and shows that the results derived from Figure 8 may be generalized to all sites except those of Arabia (peak-to-peak relative variations reaching 53%), again quite likely because of their relatively high associated view zenith angle.

The directional signature obtained in Figure 8 is qualitatively similar to bare soil directional signatures measured on the ground. The reflectance increases as expected with θ_S. Moreover, Figure 8 shows that for a given θ_S, the reflectance is generally higher when the relative azimuth φ decreases, which is again an expected behavior since bare soils usually have a higher reflectance in the backscattering half-space than in the forward scattering half-space (e.g., Kimes, 1983; Cosnefroy et al., 1996). The observed directional features are also consistent with previous satellite observations of desert areas showing an enhancement of reflectance in the backscattering region, using AVHRR/NOAA (e.g., Staylor, 1990; Santer and Roger, 1993) or ERB[11]/Nimbus 7 (Staylor and Suttles, 1986).

The results of a least-squares fit between the data and the model of Eq. (2) are shown in Table 3 (columns f and g) in a format identical to the results of Table 3 (columns b and c) obtained with the seasonal data set. The rms differences between modeled and observed reflectances, expressed in relative values, are in the range 0.5–2% in all cases. As above, these numbers may be considered as an order of magnitude estimate of temporal instabilities in reflectances at short time scales (or perhaps an upper limit of this magnitude, if we account for the fact that the directional model may not be perfectly suited to the data). The associated R^2 coefficients are in most cases larger than 0.8.

Comparison between Directional Models Associated with Seasonal and Hourly data Sets

The latter results suggest the idea that most of the observed temporal variations are indeed controlled by directional effects. Some evidence supporting this statement is derived from the following.

One may compare the two time profiles of reflectances modeled for the seasonal data set, where the parameters Y_0, Y_1, N, and C_{SW} are those derived either from the fit between the model and the seasonal data set, or between the model and the hourly data set of 30 September. Figure 9 illustrates this comparison for

[11] Earth Radiation Budget.

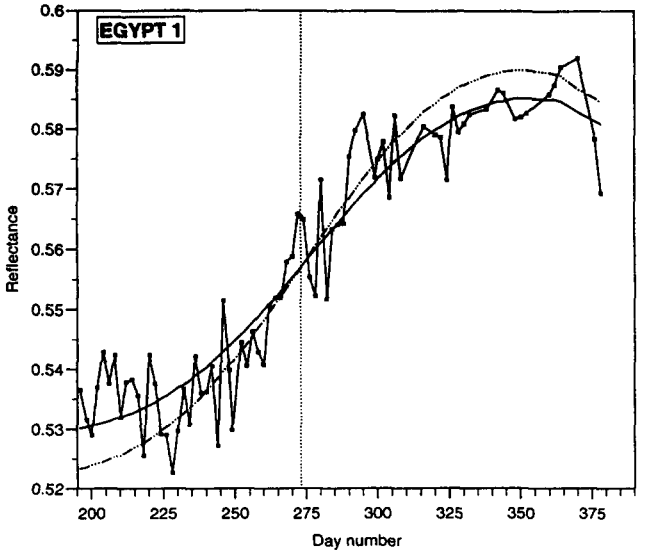

Figure 9. Broken line: seasonal evolution of spatially averaged TOA reflectance of the Egypt 1 site. Full continuous line: directional model of Eq. (1), with parameters derived from a regression between model and seasonal data set. Dashed line: the same, but where the parameters are derived from a regression between model and hourly data set.

the site Egypt 1. Such a comparison is meaningful because the range of variables θ_S and φ is significantly different in the two data sets (Fig. 10).To account for a possible bias affecting the day 30 September (the atmospheric conditions for that particular date may be slightly different from the seasonal average), a multiplicative factor, in practice close to 1, has been applied to the modeled time profile of the hourly data set so that both modeled profiles coincide on 30 September (see Fig. 9). When this is done, the rms differences between the two modeled time profiles of reflectances of each site, expressed in relative values, are shown in Table 3 (column i). This table shows that for 13 cases out of 17, the rms differences are remarkably small, less than 1%. We consider this result as a proof that most of the detected low frequency temporal variations are due to directional effects. For four cases out of 17, the rms differences range from 3% to 6% and cannot be considered as small (see Table 3, column i). We do not have any straightforward explanation for these four cases. A possibility is that the dynamic range of variations of θ_S and φ in seasonal variations is sometimes not sufficient to derive the model parameters with good accuracy. Another possibility is that the bidirectional reflectance model may not be completely adequate to describe the bidirectional reflectance properties of some of our selected sites.

CONCLUSION

Twenty different sites 100×100 km^2 in size were selected for satellite sensor calibration purposes in desertic areas of North Africa and Saudi Arabia. The sites were selected on the basis of good spatial uniformity (less than 3% in relative value) using a multitemporal series of Meteosat-4 images. This procedure has been validated, at least on a few selected sites and for short periods of time, by showing that the most spatially uniform sites are also the most stable temporally. The site characterization in terms of cloud cover and precipitation level has shown as expected that these sites are among the most easily accessible sites by satellite, and among the driest sites in the world. The geomorphological analysis of the sites using HRV / Spot images has demonstrated that most sites are made of vegetation-free sand dunes with well characterized dimensions and reliefs. Peak-to-peak amplitude of variations in reflectance due to directional effects, either with seasonal or hourly variations, have been shown to be on the order of 8–15% in relative value. A simple 4-parameter bidirectional reflectance model satisfactorily accounts simultaneously, for most sites, for the seasonal and the hourly variations in reflectance. Once the directional effects are removed, the residual rms variations, representative of random temporal variability of the spatially averaged TOA reflectance, are generally on the order of 1–2% in relative value.

As emphasized in the Introduction, the site selection process described here is a first step in the development of an operational calibration procedure routinely using desert test sites. The results presented in this article are encouraging and open interesting perspectives on the development of new calibration procedures for optical satellite sensors. The sites have a very good

Figure 10. Polar representation of the θ_S and φ variations of the Meteosat-4 seasonal (full line) and hourly (triangles) data sets, for the Egypt 1 site. The radius and polar angle represent respectively θ_S and φ. The radius of the icone on the $\varphi = 0$ axis represents the viewing zenith angle.

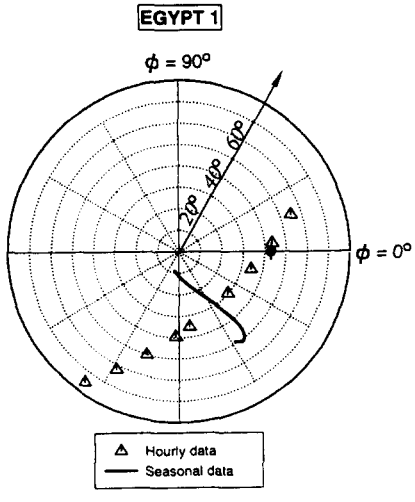

performance of temporal variability (1–2%). This performance includes the variability of the surface and of the atmosphere. The contribution of this performance to the calibration error budget depends on the number of satellite calibrations that are completed. An individual satellite calibration experiment would be affected by the totality of this error. On the other hand, by averaging the results of a large number of calibration experiments (very easy to perform in practice, since the temporal repetitiveness of satellite observations is usually high), one can make this contribution to the error budget virtually disappear.

Metrological measurements of TOA bidirectional spectral reflectance of the sites are the second step of the development of our calibration procedure. An investigation program has begun, which has included so far a dedicated airborne campaign on one selected site in the Ténéré (Niger 1) in October 1992 with the airborne version of the POLDER instrument, and a field campaign performed at four selected sites in Algeria in February–March 1993 (Cosnefroy et al., 1996). The errors associated with the measurement of the spectral and directional variations of site reference reflectance are the second important class of errors, the first one being that of the site temporal variability. The magnitude of these errors can be estimated using the results of the campaigns of Niger and Algeria, and will be presented in forthcoming publications.

The authors are indebted to G. Sèze, M. Desbois (Laboratoire de Météorologie Dynamique, Palaiseau), and Y. Dupuis (Centre National d'Etudes Spatiales, Toulouse) for kindly providing relevant ISCCP C1 data. They also wish to thank P. Bicheron (Laboratoire d'Etudes et de Recherches en Télédétection Spatiale, Toulouse) for the processing of Spot images. These Spot data have been acquired in the context of the ISIS program (Incitation à l'utilisation Scientifique des Images Spot). This study has been funded by Centre National d'Etudes Spatiales. The authors finally thank an unknown reviewer for numerous editorial suggestions and English corrections.

REFERENCES

Cabot, F., Dedieu, G., and Maisongrande, P. (1994), Monitoring NOAA / AVHRR and Meteosat shortwave bands calibration and intercalibration over stable areas, in *Proc. 6th ISPRS Int. Symp. on Phys. Measurements and Signatures in Remote Sensing*, Val d'Isère, France, CNES, Toulouse, pp. 41–46.

Capderou, M., and Kandel, R. (1994), Clear-sky criteria and cloud cover over desert areas from Meteosat data, *J. Appl. Meteorol.* 33(4):546–567.

Cooke, R. U., Warren, A., and Goudie, A. S. (1993), *Desert Geomorphology*, UCL Press, London.

Cosnefroy, H., Briottet, X., Leroy, M., Lecomte, P., and Santer, R. (1996), A field experiment in Sahara for the calibration of optical satellite sensors, *Int. J. Remote Sens.* (in press).

Dedieu, G. (1992), Surface radiation budget in the shortwave using the Meteosat ISCCP-B2 dataset, in *Proc. 9th Meteosat Scientific User Meeting*, EUM P 11, EUMETSAT Editor, Locarno, Suisse, pp. 69–76.

Delphin, L., Briottet, X., Vermote, E., and Leroy, M. (1991), Caractérisation de sites désertiques Africains pour l'étalonnage relatif des capteurs optiques spatiaux à grand champ, in *Proc. 5th ISPRS Int. Symp. on Phys. Measurements and Signatures in Remote Sensing*, Courchevel, France, ESA SP-319, Paris, pp. 49–52.

Deschamps, P. Y., Bréon, F. M., Leroy, M., et al. (1994), "The POLDER MIssion: instrument characteristics and scientific objectives, *IEEE Trans. Geosci. Remote Sens.* 32(3):598–615.

Gastineau, J. (1991), Suivi de l'étalonnage du canal des courtes longueurs d'onde de Meteosat, Rapport de stage de DESS, Université Paul Sabatier, available from CESBIO, Toulouse, France.

Henry, P., Dinguirard, M., and Bodilis, M. (1993), Spot multitemporal calibration over stable desert areas, *SPIE Int. Symp. Aerospace and Remote Sensing*, Technical Conference 1938, 12–16 April, Orlando, pp. 67–76.

Holben, B. N., Kaufman, Y. J., and Kendall, J. D. (1990), NOAA-11 AVHRR visible and near infrared inflight calibration, *Int. J. Remote Sens.* 11:1511–1519.

Jaccoberger, P. A. (1989), Reflectance characteristics and surface processes in stabilized dune environments, *Remote Sens. Environ.* 28:287–295.

Kaufman, Y. J., and Holben, B. N. (1993), Calibration of the AVHRR visible and near-IR bands by atmospheric scattering, ocean glint and desert reflection, *Int. J. Remote Sens.* 14:21–52.

Kimes, D. S. (1983), Dynamics of directional reflectance factor distribution for vegetation canopies, *Appl. Opt.* 22(9): 1364–1372.

Kriebel, K. T., and Amann, V. (1993), Vicarious calibration of the Meteosat visible channel, *J. Atmos. Ocean. Technol.* 10:225–232.

Mainguet, M. A. (1984), A classification of dunes based on aeolians dynamics and the sand budget, in *Desert and Arid Lands*, Collection Remote Sensing of Earth Resources and Environment (F. El-Baz, Ed.) Martinus Nijhoff, The Hague, pp. 31–58.

Rossow, W. B. (1989), Measuring cloud properties from space: a review, *J. Clim.* 2:201–213.

Rossow, W. B., and Schiffer, R. A. (1991), ISCCP C1 cloud data products, *Bull. Am. Meteorol. Soc.* 115:551–572.

Rossow, W. B., Gardner, L. C., Lu, P. J., and Walker, A. (1988), International satellite cloud climatology project (ISCCP) documentation on cloud data, WMO / TD No. 266, World Meteorological Organisation, Geneva, Switzerland, 78 pp. + 2 appendices.

Santer, R., and Roger, J. C. (1993), NOAA-11 Channels 1 and 2 calibration in the SPACE software, in *SPIE Int. Symp. in Aerospace and Remote Sensing*, Technical Conference 1938, 12–16 April, Orlando, pp. 77–85.

Santer, R., Asmani, M., Vermote, E., and Sharman, M. (1991), Inflight calibration of Channels 1 and 2 of AVHRR using desertic sites and clouds, in *Proc. 5th ISPRS Int. Symp. on Phys. Measurements and Signatures in Remote Sensing*, Courchevel, France. pp. 65–68.

Santer, R., Gu, X. F., Guyot, G., et al. (1992), SPOT calibration at La Crau test site, *Remote Sens. Environ.* 41:227–237.

Schiffer, R. A., and Rossow, W. B. (1983), The International Satellite Cloud Climatology Project (ISCCP)—the first project of the World Climate Research Program, *Bull. Am. Meteorol. Soc.* 64:779–784.

Slater, P. N., Biggar, S. F., Holm, R. G., et al. (1987), Reflectance and radiance-based methods for the in-flight absolute calibration of multispectral sensors, *Remote Sens. Environ.* 22:11–37.

Staylor, W. F. (1990), Degradation rates of the AVHRR visible channel for the 6, 7, and 9 spacecraft, *J. Atmos. Ocean. Technol.* 7:411–423.

Staylor, W. F., and Suttles, J. T. (1986), Reflection and emission models for deserts derived from Nimbus ERB scanner measurements, *J. Clim. Appl. Meteorol.* 25:196–202.

Teillet, P. M., Slater, P. N., Mao, Y. (1990), Three methods for the absolute calibration of the NOAA AVHRR sensors in flight, *Remote Sens. Environ.* 31:105–120.

Vose, R. S., Schmoyer, R. L., Steurer, P. M., et al. (1992), The global historical climatology network: long-term monthly temperature, precipitation, sea level pressure, and station pressure data, *Environmental Sciences Division Publication* No. 3912, Oak Ridge National Laboratory, Oak Ridge, TN.

Wheeler, R. J., LeCroy, S. R., Whitlock, C. H., Purgold, G. C., and Swanson, J. S. (1994), Surface characteristics of the Alkali Flats and dune regions at White Sands Missile Range, New Mexico, *Remote Sens. Environ.* 48:181–190.